PHYSICAL REVIEW B VOLUME 25, NUMBER 2 15 JANUARY 1982

Surface electronic structure of rhodium (100)

J. G. Gay, J. R. Smith, and F. J. Arlinghaus
Physics Department, General Motors Research Laboratories, Warren, Michigan 48090
(Received 10 August 1981)

The electronic structure of the (100) surface of rhodium has been calculated theoretically using the self-consistent local-orbital method. As in our earlier calculations on d-band metal surfaces [Cu(100), Ni(100), Pd(100), and Ag(100)] we find a large percentage of the surface electrons of Rh(100) are in surface states. In addition to presenting the band structure and total densities of states (DOS), we analyze the Rh(100) electronic structure in a new fashion by calculating annular densities of states. These annular densities of states, which are the appropriate quantities to compare with photoemission data collected by cylindrical mirror analyzers (CMA), show distinctive features related to the restricted regions of $\vec{k}_{||}$ space which they sample. The results suggest that considerable care must be taken in comparing CMA spectra with DOS. $\vec{k}_{||}$-selected densities of states (DOS) are given for $\vec{k}_{||}$ along the $\bar{\Gamma}-\bar{X}[110]$ and $\bar{\Gamma}-\bar{M}[100]$ directions. The strong variation of the $\vec{k}_{||}$-selected DOS with $\vec{k}_{||}$ shows that a large part of the variation of surface-state peak heights with angle in angular photoemission can be due to initial DOS variation. The strong DOS variation with mirror plane symmetry shows that it is important to use polarized light.

I. INTRODUCTION

As part of a continuing study of the electronic structure of d-band metal surfaces we have carried out a calculation of the electronic structure of Rh(100) using our self-consistent local-orbital (SCLO) method. In previous calculations on Cu(100),[1,2] Ni(100),[3] Ag(100),[4] and Pd(100),[5] we found that substantial fractions of the surface layer electrons occupied surface states or surface resonances. A similar situation is found also for Rh(100), and we have been able to show a correlation between the fraction of electrons in surface states in the surface layer and surface potential shifts.[6] Here we describe and present the results of the Rh(100) calculation. In Sec. II we give a brief account of the calculational method and present the electronic structure of Rh(100) in the form of the two-dimensional band structure with surface states delineated, and planar and total densities of states (DOS). In Sec. III we present the $\vec{k}_{||}$-selected densities of states[5] of Rh(100) and in Sec. IV we calculate for the first time densities of states selected from annular rings in reciprocal space. These ring DOS select those initial states which contribute to the signal collected by a cylindrical mirror analyzer with its axis perpendicular to the sample surface.

II. Rh(100) ELECTRONIC STRUCTURE

The SCLO method, as applied to Cu(100), has been described in detail.[2] Rh is a 4d metal and therefore requires a larger number of more complex atomic orbitals than does the 3d metal Cu. In fitting the atomic orbitals, we used 13 s-type, 9 p-type, and 7 d-type Gaussian orbitals; the same as for Pd and Ag and two more of each angular momentum type than for copper. The 5p, 5d, and 6s orbitals were constructed exactly as the 4p, 4d, and 5s orbitals were for copper. The atomic potential fits used 16 instead of 14 Gaussians. In the atomic calculation upon which these fits were based we used a $4d^8 5s^1$ configuration. The 3d and 4d metal calculations are analogous in other respects. The same number of components are used in the Fourier transforms and the mesh size used in computing transforms of the difference charge density was again chosen to be $\frac{1}{10}$ of the lattice constant.

For Cu(100) and Ni(100) we used a nine-plane slab to ensure a slab sufficiently thick to study surface states. However, comparison of seven- and nine-plane results for Cu(100) has convinced us that seven planes gives essentially the same surface-state density as nine planes. Accordingly, as a matter of economy, we have chosen to limit

the 4*d* metal slabs to seven planes.

We initiated the seven-plane calculation by carrying out a three-plane calculation. The self-consistent charge density for this calculation was used, as described in Ref. 1, to generate a starting charge density for the seven-plane slab. Initially, during iteration to self-consistency, we used 6 $k_{||}$ points in the irreducible part of the Brillouin zone to construct corrections to the charge density. We found that after the calculation had converged to a point where the maximum difference between input and output potentials was about 0.5 eV the system entered a bistable mode in which two states near the Fermi level alternately rose and fell below the Fermi level on successive iterations. The bistable mode was persistent upon continued iteration. We then increased the number of $k_{||}$ points to 15 and began a new iteration sequence. After converging to about 150 mV everywhere in the unit cell, this sequence entered a similar bistable mode which was also persistent. We then examined the electronic structure of two successive iterations by solving for the eigenstates at 45 $k_{||}$ points in the irreducible zone using potentials from the two iterations. We found the two electronic structures identical in the sense that densities of states and band structures (e.g., Figs. 1 and 2) were indistinguishable and the electron work functions were the same. On the basis of this result we conclude that the calculation was sufficiently converged.

Densities of states (DOS) for Rh are shown in Fig. 1. In general shape and width our planar[2] DOS for the central plane and our total DOS for the seven-plane slab agree well with the bulk DOS of Rh computed by Moruzzi, Janak, and Williams.[7] Both should converge, in the limit of a large number of planes, to the bulk DOS which would result from using our basis set in a bulk calculation. The *d* band of Rh is substantially wider than the *d* band of Pd (Ref. 5) which, in turn, is wider than that of Ag.[4] The surface plane DOS shows this widening but also shows the narrowing, compared to the bulk, which is observed in all our calculations and which is due to the fewer neighbors seen by atoms in the surface plane.

Figure 2 shows the two-dimensional band structure of the slab along high-symmetry directions in the Brillouin zone. Surface states and resonances are indicated by open circles. These were selected by the criterion discussed in Ref. 5 which requires that at least 80% of the states charge density reside on the surface plane and the plane beneath it.

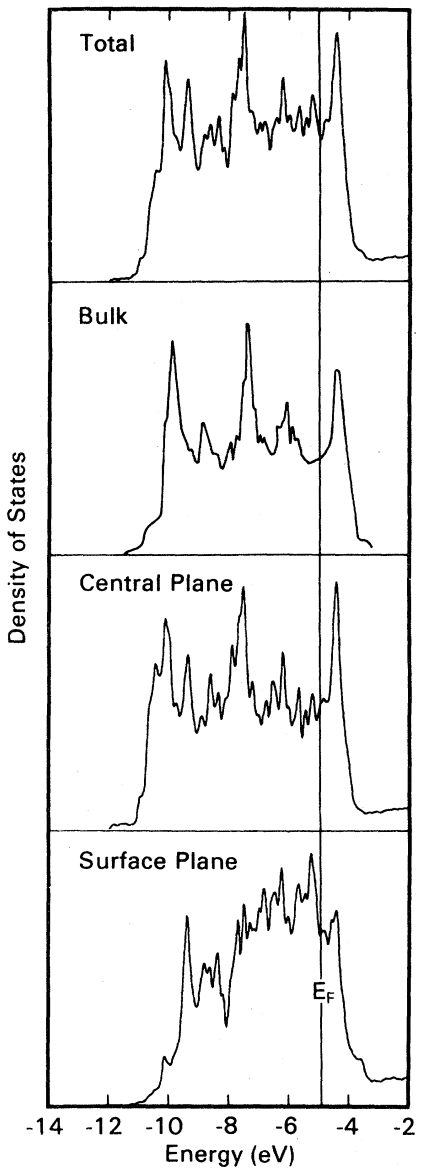

FIG. 1. Density-of-states curves for the seven-plane Rh(100) film. The bulk density of states was taken from Ref. 7.

The surface states are concentrated somewhat toward the top of the *d* band, as we have found previously for Ni and Pd, but are not so concentrated there as we have observed for the noble metals Cu and Ag. Nevertheless, Rh(100) has as large a fraction of its surface plane electrons in surface states (23%) as any of the metals we have studied save Cu. The metals in order of decreasing surface-state fraction are Cu (36%), Rh (23%), Ni (23%), Ag (22%), and Pd (19%).

We obtain a work function of 4.8 eV for

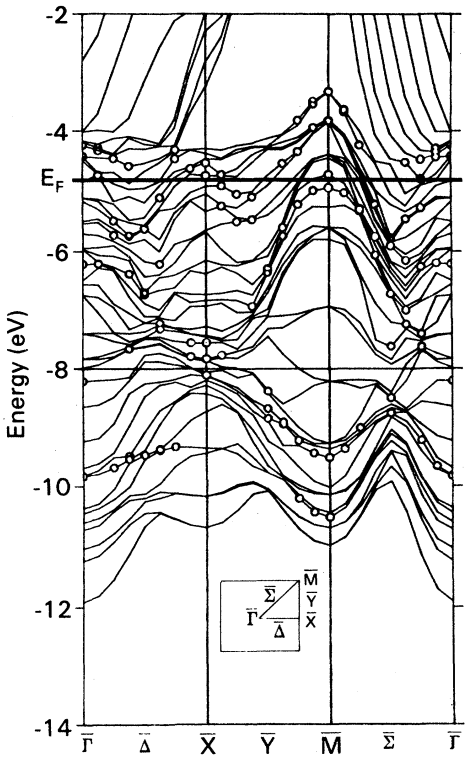

FIG. 2. Surface band structure along high-symmetry directions for the seven-plane Rh(100) slab. The open circles represent states on the 45 $\vec{k}_{||}$-point mesh which are highly localized in the surface plane of the slab.

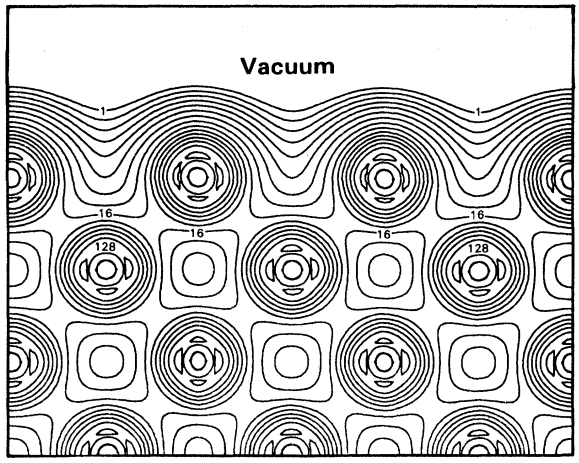

FIG. 3. Self-consistent conduction-band electronic charge density for a seven-layer Rh(100) film plotted on a plane perpendicular to the surface and passing through a line connecting a surface atom with one of its near neighbors in the second plane of atoms. The units of charge density are 3.44×10^{-3} a.u. Charge densities on successive contours are in the ratio $\sqrt{2}$. The small hemispherical contours in the *d*-electron region at each atomic site enclose local maxima in the charge density.

Rh(100). To our knowledge no experimental determination has been reported. Work functions from our previous calculations have been accurate to within 0.3 eV.

Contours of the self-consistent Rh(100) conduction-band change density are plotted in Fig. 3. The contours give the density in a plane perpendicular to the surface and passing through nearest-neighbor atoms in adjacent planes. The unfilled *d* band is reflected in the evident lack of spherical symmetry in the *d*-electron change density. Also notable is the marked similarity of the surface plane and interior plane *d*-electron change densities.

Owing to a programming error which produced a spurious exchange-correlation potential, an initial calculation[6] for Rh(100) was slightly in error. The principal differences between those Rh(100) results in Ref. 6 and the results reported here are that the *d* bands were 5% wider, and 27% of the surface plane electrons were in surface states compared with 23% reported here.

We reported in Ref. 6 core shifts evaluated at $\bar{\Gamma}$. We have found for the 4*d* metals, however, that the highest core levels exhibit non-negligible bandwidths (up to 0.2 eV). The correlation with surface-state densities discussed in Ref. 6 still holds if one uses average core band energies, however. The physical basis of the correlation is that there is an average upward shift of the potential in going from bulk sites to surface sites. A more accurate measure of this shift is to take the difference between the diagonal potential matrix elements of the spherically symmetric 4*s* core orbitals on the central and surface planes. When this is done we find the matrix-element differences to be Rh (0.52 eV), Ag (0.50 eV), and Pd (0.39 eV) which correlate well with the surface-state fractions which are Rh (23%), Ag (22%), and Pd (19%).

III. $\vec{k}_{||}$-SELECTED DENSITIES OF STATES

The DOS of Fig. 1 are obtained from a uniform average over the two-dimensional Brillouin zone. In angle-resolved ultraviolet photoemission (ARUP) experiments, however, the initial states which contribute to the photoemission signal all lie in a small region of the zone centered at some $\vec{k}_{||}$.

In Ref. 5 we have described a procedure for computing $\vec{k}_{||}$-selected DOS, i.e., DOS arising from states located in a small square centered at some $\vec{k}_{||}$, and have discussed their relation to ARUP data.

$\vec{k}_{||}$-selected DOS have previously been calculated for Ag(100) (Ref. 4) and Pd(100).[5] We follow the same procedure that was used in those calculations and present $\vec{k}_{||}$-selected DOS along the high-symmetry directions $\bar{\Gamma}$-$\bar{M}$ and $\bar{\Gamma}$-$\bar{X}$ for Rh(100). For $\vec{k}_{||}$ vectors along these mirror plane directions, the wave functions are either even or odd with respect to mirror plane reflection. We compute DOS for each symmetry because they can be separated experimentally using polarized light in angular photoemission. Also, we can determine projections of $\vec{k}_{||}$-selected DOS on atomic planes. This allows one to identify peaks associated with surface-state bonds. Direct transition effects will cause measured spectra to look somewhat different from the DOS. This will not be true for surface-state or adsorbate bands. Surface states are difficult to find experimentally on metals because there is no bulk band gap. Locating surface-state peaks in $\vec{k}_{||}$-selected DOS may facilitate their location in angular photoemission spectra. The identification of a peak in a photoemission spectrum as being due to a surface-state band can be checked by varying the photon energy and making sure the peak does not shift in energy. This applies equally to the identification of adsorbate bands.

In Figs. 4—7 we present (occupied) $\vec{k}_{||}$-selected DOS along the mirror plane directions projected on the central plane of the slab and projected on the surface plane of the slab. The central plane projections represent bulk contributions, while the surface plane projections emphasize surface-state contributions.

These figures show that there are similarities between the central plane results, which are representative of the bulk, and the surface plane results. There are also marked differences which are primarily due to surface states. In Figs. 5 and 7 we have noted with arrows peaks in the surface plane DOS which are much smaller in the central or are not present at all. We hope that identifying surface-state features in the DOS in this manner will help experimentalists isolate surface-state bands. Once candidate peaks are observed in the appropriate energy and momentum range, they may be confirmed as surface features by varying the photon energy and making certain these peaks do not disperse with $k_\perp$.

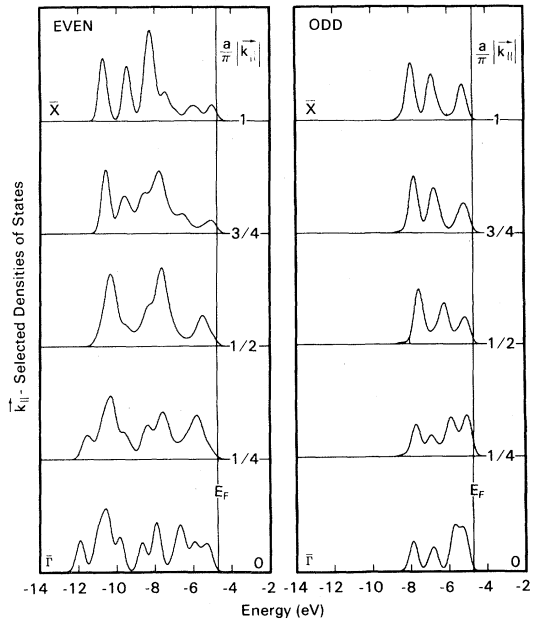

FIG. 4. $\vec{k}_{||}$-selected densities of states for Rh(100) central plane, (100) azimuth.

IV. ANNULAR DENSITIES OF STATES

The DOS presented in Sec. II are a uniform average over electron states in $\vec{k}_{||}$ space. It is common to compare such DOS with angle-averaged

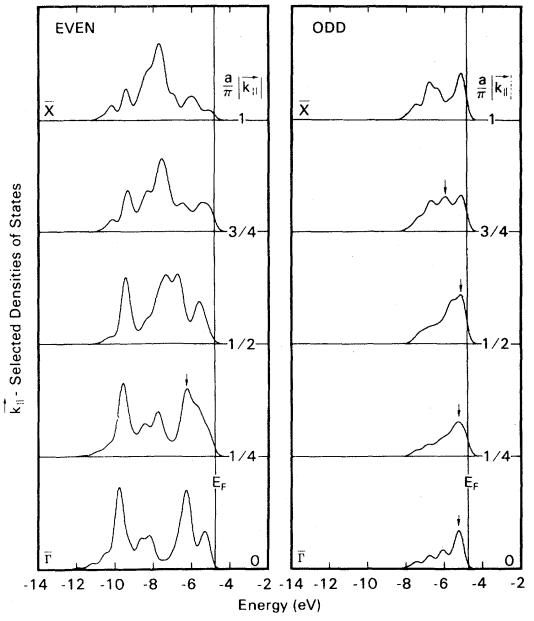

FIG. 5. $\vec{k}_{||}$-selected densities of states for Rh(100) surface plane, (100) azimuth. The arrows indicate peaks which either do not exist in the central (bulk) plane, or are much smaller there.

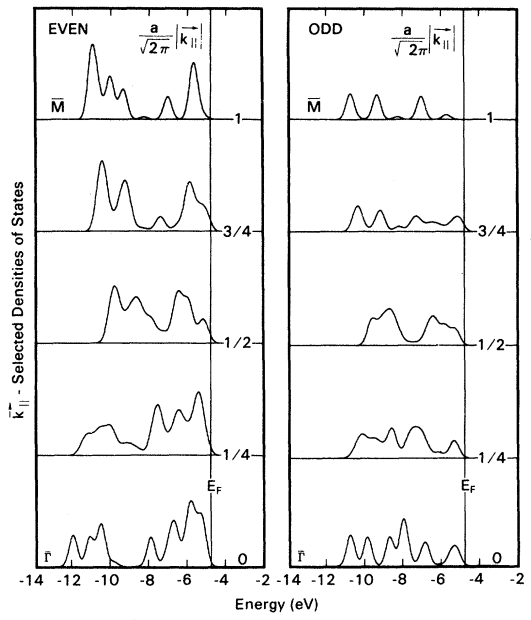

FIG. 6. $\vec{k}_{||}$-selected densities of states for Rh(100) central plane, (110) azimuth.

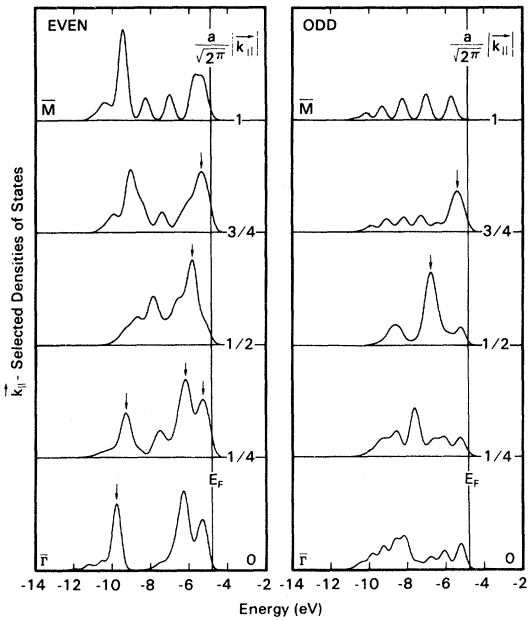

FIG. 7. $\vec{k}_{||}$-selected densities of states for Rh(100) surface plane, (110) azimuth. The arrows indicate peaks which either do not exist in the central (bulk) plane, or are much smaller there.

photoemission spectra obtained with cylindrical mirror analyzer (CMA) detectors. These comparisons are not really appropriate since the initial states which contribute to the CMA signal lie in annular region of $\vec{k}_{||}$ space which depends on the orientation of the analyzer axis relative to the surface normal.

In this section we compute annular DOS for Rh(100) which correspond to the regions of $\vec{k}_{||}$ space sampled by the popular physical electronics double-pass CMA oriented with its axis normal to the surface and operating at 16.7-, 21.2-, and 40.8-eV photon energies. The physical electronics CMA at narrow aperture, when oriented with its axis normal to the surface, accepts electrons with $\vec{k}$ vectors lying outside a cone with normal axis and generating angle of 39.3°, and inside a cone with normal axis and generating angle 45.3°. For electrons of initial energy E_I the region of $\vec{k}_{||}$ space which contributes to the CMA signal is an annular ring centered at the origin with inner boundary of radius

$$k_{\min}=[2(h\omega+E_I)]^{1/2}\sin(39.3^\circ) \tag{1}$$

and center boundary of radius

$$k_{\max}=[2(h\omega+E_I)]^{1/2}\sin(45.3^\circ)\,, \tag{2}$$

where $h\omega$ is the photon energy. In (1) and (2) energies are measured in Hartrees.

The rings which correspond to 16.7-, 21.2-, and 40.8-eV photons and a midband E_I of -7 eV are shown in Fig. 8 along with their mappings into the first Brillouin zone. The annular DOS are computed using a Monte Carlo technique.[2] Random points, chosen uniformly over the first two Brillouin zones, are mapped, if necessary, into the equivalent points inside the first Brillouin zone. Quadratic interpolation is used to determine the eigenvalues from the previously tabulated solutions at 45 regularly spaced points covering the irreducible $\frac{1}{8}$ of the Brillouin zone. Each energy thus obtained is substituted into (1) and (2) and only those states are kept which fall inside the annular ring thus defined. The density of such states is then constructed as described in Ref. 2.

Annular DOS for the seven-plane slab and the three-photon energies are shown in Fig. 9. Marked deviations from the total DOS of Fig. 1 are apparent in the 16.7- and 21.2-eV spectra whereas the 40.8-eV DOS is much more like the total. This is basically a consequence of the fact that the annulus area increases with photon energy coupled with the fact that, at higher energies, mapping back into the

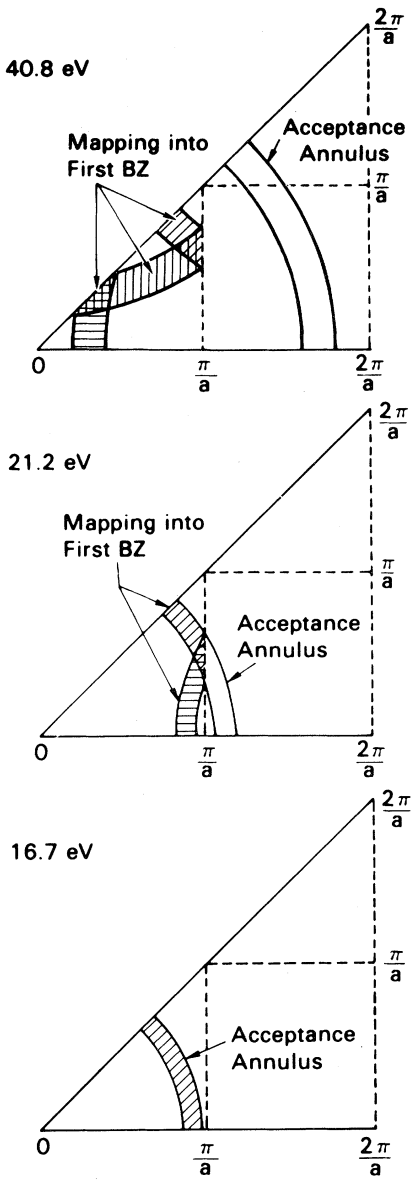

FIG. 8. Annular regions of $\vec{k}_{||}$ space from which electrons collected by a CMA analyzer originate. The regions are shown for three-photon energies with a initial state energy of -7 eV. Shaded regions are mappings of the annuli into the first Brillouin zone.

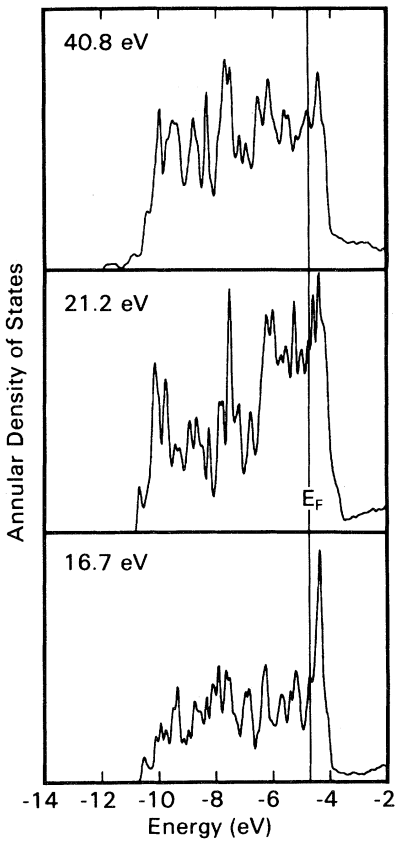

FIG. 9. Annular DOS for the three-photon energies.

first Brillouin zone tends to cause the zone to be sampled more uniformly. These two effects are manifest in Fig. 9. Another effect is that, for fixed photon energy, the annular area decreases as the initial state energy decreases producing a tendency toward decreasing DOS magnitude with decreasing initial energy. This may be the reason the 40.8-eV DOS has an overall "trapezoidal" shape in contrast to the "rectangular" shape of the total DOS. The effect increases with decreasing photon energy and therefore is operative at the two lower photon energies. For these, however, the effort may be masked by the highly nonuniform sampling of the Brillouin zone. For both lower energies, the region at the zone near $\bar{\Gamma}$ is not sampled, leading to a complete absence of *s*-electron density below the *d* band.

The above results show that the effects of nonuniform sampling by CMA detectors qualitatively affects the density of initial states which contribute to the photoemission signal and should be taken into account in comparing theory and experiment, particularly at low photon energies.

When certain spectral features originate from localized regions of the Brillouin zone the CMA may miss them entirely. An example is the predicted surface state at $\bar{M}$ in Cu(100) (Refs. 1 and 2) which was subsequently seen in ARUP experiments.[8–11] It, however, would not contribute to the signal of a

CMA when oriented with its axis normal for the three energies considered above since $\bar{M}$ is not sampled under these conditions.

We note finally that normal orientation of a CMA produces the most localized sampling of the Brillouin zone since each irreducible octant is sampled identically. Nonnormal orientation will cause the octants to be sampled differently thus producing a less-localized sampling.

Note added in proof. Subsequent to the completion of this calculation, Galen B. Fisher measured the work function of Rh(100). His value of 4.6 ± 0.1 eV is in good agreement with our predicted value of 4.8 eV.

ACKNOWLEDGMENT

We wish to thank Galen B. Fisher for suggesting that we consider the effects of nonuniform sampling of the Brillouin zone by CMA detectors.

[1]J. G. Gay, J. R. Smith, and F. J. Arlinghaus, Phys. Rev. Lett. 42, 332 (1979).

[2]J. R. Smith, J. G. Gay, and F. J. Arlinghaus, Phys. Rev. B 21, 2201 (1980). For comparisons of our method with those of other workers, see *Topics in Current Physics, Theory of Chemisorption,* edited by J. R. Smith (Springer, New York, 1980), Vol. 19, Chap. 4; and J. R. Smith, F. J. Arlinghaus, and J. G. Gay, J. Vac. Sci. Technol. 18, 411 (1980).

[3]F. J. Arlinghaus, J. G. Gay, and J. R. Smith, Phys. Rev. B 21, 2055 (1980).

[4]J. R. Smith, F. J. Arlinghaus, and J. G. Gay, Phys. Rev. B 22, 4757 (1980).

[5]J. G. Gay, J. R. Smith, F. J. Arlinghaus, and T. W. Capehart, Phys. Rev. B 23, 1559 (1981).

[6]F. J. Arlinghaus, J. R. Smith, and J. G. Gay, Phys. Rev. B 23, 5152 (1981).

[7]V. L. Moruzzi, J. F. Janak, and A. R. Williams, *Calculated Electronic Properties of Metals* (Pergamon, New York, 1978), p. 145.

[8]P. Heimann, J. Hermanson, H. Miosga, and H. Neddermeyer, Phys. Rev. Lett. 42, (1979).

[9]P. Heimann, J. Hermanson, H. Miosga, and H. Neddermeyer, Phys. Rev. B 20, 3059 (1979).

[10]S. D. Kevan and D. A. Shirley, Phys. Rev. B 22, 542 (1980).

[11]D. Westphal and A. Goldmann, Surf. Sci. 95, L249 (1980).